J Mater Sci: Mater Electron (2017) 28:7943–7950
DOI 10.1007/s10854-017-6496-3

Preparation and photocatalytic properties of hexagonal-shaped ZnO:Sm^{3+} by microwave-assisted hydrothermal method

R. G. Carvalho[1] · M. T. S. Tavares[2] · F. K. F. Oliveira[1] · R. M. Nascimento[1] · E. Longo[3] · M. S. Li[4] · C. A. Paskocimas[1] · M. R. D. Bomio[1] · F. V. Motta[1]

Received: 16 October 2016 / Accepted: 30 January 2017 / Published online: 9 February 2017

Abstract Novel 3D rods ZnO:Sm monophasic microcrystals have been synthesized by the microwave-assisted hydrothermal (MAH) method at 140 °C for 10 min. The experimental results revealed that concentration of samarium have a significant influence on the band gap and photocatalysis. On the other hand, the samarium in the ZnO semiconductor structure increases photodegradation activity. ZnO sample doped with 8% Sm^{3+} exhibited the best activity in the photodegradation of methylene blue dye when compared to that doped with 0–4 mol%. Enhanced photocatalytic activity was attributed to samarium, which inhibits the recombination of electron–hole pairs.

1 Introduction

ZnO has been used in research on decomposing organic pollutants and in the sterilization of materials for killing bacteria [1–3]. The disadvantage in the use of ZnO as a commercial photocatalyst is its band gap of 3.3 eV, so the ZnO activity is limited to the ultraviolet region. Another problem is the recombination of photogenerated charges (electron–hole) that decreases the photocatalytic efficiency of the process [4–8]. In order to meet the environmental protection requirements, there is a great challenge for researchers who try to improve the photocatalytic property of ZnO, which is highly efficient in the degradation of waste from the textile industry. Some studies have reported that rare earth ions are useful to overcome the disadvantages of ZnO [9–13]. The incorporated rare earth ions in the host matrix are expected to introduce structure defects and thereby the formation of intermediary energy levels inside of the band gap. This behavior is related the doping of rare earth ions can form traps for decreased the electron–hole pairs recombination rate [10]. Zhou et al. [14] investigated the photocatalytic activity of Nd-doped ZnO with different Nd mol% and the result of the solution pH in the degradation of C.I. Reactive Blue 4. It was observed that the degradation rate of Nd-doped ZnO increases the load in 2.5 mol% Nd with pH 11, approximately.

Vignesh et al. [15] investigated the photocatalyst activity of Th–ZnO–Ni in methylene blue (MB) and showed that Th degradation enhances the activity of this photocatalyst. Faisal et al. [16] showed the photocatalytic activity of Ce-doped ZnO nanorods prepared by hydrothermal method. The degradation rates for MB decomposition were found to increase linearly with the increase in Ce contents from 0 to 0.5% molar ratio and from this point, they decrease.

Recently, samarium-doped ZnO was synthesized via solvothermal method and showed the photocatalytic degradation of the phenol aqueous solution [17]. Moreover, the photocatalytic activity of Sm-doped ZnO synthesized by the wet chemical route was measured by the degradation of blue acid 113 [18]. However, there are no studies on the photocatalytic degradation of methylene blue by samarium-doped ZnO powders in literature.

Several synthesis methods to produce ZnO nanostructures doped with rare earth have been reported, including

✉ F. V. Motta
fabiana@ct.ufrn.br

[1] LSQM, DEMAT, UFRN, Av. Sen. Salgado Filho, 3000, Natal, RN CEP 59072-970, Brazil

[2] IFBA, Campus Feira de Santana, Bahia, BA CEP 44096-486, Brazil

[3] LIEC, DQ, UFSCar, Via Washington Luiz, km 235, São Carlos, SP CEP 13565-905, Brazil

[4] IFSC, USP, Av. Trabalhador São Carlense, 400, São Carlos, SP CEP 13566-590, Brazil

hydrothermal method [19, 20], precipitation [21], microwave irradiation [22], chemical vapor deposition [23] and ultrasound [24].

Hydrothermal synthesis using microwaves is a method that has shown great potential as it allows a better control over the phases formed, rapid heating and shorter reaction time. In this study, ZnO:xSm^{3+} (x = 0, 1, 2, 4 and 8 mol%) was prepared by MAH method at low time for 10 min at 140 °C. Methylene blue dye was used as pollutant degradation in the test, being a product widely used in the textile industry. The influence of the Sm^{3+} ion content on the photocatalytic activity and its structural characterization were investigated.

2 Experimental procedures

2.1 Synthesis of ZnO:Sm^{3+} powders

ZnO:Sm^{3+} powders were prepared by microwave-assisted hydrothermal (MAH) method. Sm^{3+} ion was added in the following percentages: 0, 1, 2, 4 and 8 mol%. Precursors $Zn(NO_3)_2{\cdot}6H_2O$ (Synth), $Sm(NO_3)_3{\cdot}6H_2O$ (Alfa Aesar), were dissolved in 80 mL deionized water under constant stirring. The solution pH was adjusted to 10 by adding NaOH. The solution was then transferred to Teflon-lined stainless steel autoclave, sealed, and placed in domestic microwave (2.45 GHz). The reaction system was heat and treated at 140 °C for 10 min at all samarium percentages investigated. Pressure of 3 kgf/cm^2 was constant inside the autoclave. Precipitates were separated by centrifugation, washed with deionized water to neutralize the solution and dried at room temperature for 24 h.

2.2 Characterization of ZnO:Sm^{3+} powders

Powders were characterized by X-ray diffraction (XRD) using Shimadzu diffractometer (Model XRD-7000, CuKα radiation (λ = 1.54 Å)). The routine was performed in the 2θ range from 10° to 80° using an angular step of 0.02°/s and total exposure time of 90 min.

The ZnO:xSm^{3+} morphology was observed by images obtained using scanning electron microscope (SEM) (Carl Zeiss, Supra 35-VP Model, Germany). UV–vis reflectance spectra of powders were performed using Shimadzu (model UV-2600) equipment. All measurements were performed at room temperature.

2.3 Photocatalytic activity measurement

The photocatalytic properties of ZnO (as a catalyst agent) for the degradation of MB (methylene blue) dye was tested with a molecular formula $C_{16}H_{18}N_3SCI$ (99.5% purity) in an aqueous solution under UV-light illumination. About 50 mg of catalyst crystals, and 50 mL of MB solution were placed in a 250 mL beaker (1×10^{-5} mol L^{-1}). These suspensions were ultrasonicated for 15 min in an ultrasonic cleaner before illumination and then stored in the dark for 5 min to allow the saturated absorption of MB onto the catalyst. Beakers were placed in a photo-reactor at controlled temperature (20 °C), under magnetic stirring and illuminated by six UVC lamps (TUV Philips, 15 W, with maximum intensity at 254 nm). At intervals of 30 min, one 1 mL aliquot of these suspensions was removed and centrifuged at 9000 rpm for 4 min to remove suspended particles. Finally, variations of the maximum absorption band of supernatant solutions were monitored by UV–visible absorbance spectra measurements using Shimadzu (model UV-2600) spectrophotometer. All measurements were performed at room temperature. Photodegradation was calculated using the expression [21] given below:

$$\text{Photodegradation \% of MB} = \frac{(C_0 - C)}{(C_0)} \quad (1)$$

where C_0 is the MB concentration before irradiation (MB concentration after 30 min adsorption in dark) and C is the MB concentration after a certain irradiation time.

3 Results and discussion

Figure 1a–e shows XRD patterns of ZnO:xSm^{3+} (x = 0, 1, 2, 4 and 8 mol%) prepared by MAH method at 140 °C for 10 min. XRD results indicate well defined diffraction peaks with high degree of crystallization, which is a characteristic of the ZnO layer with hexagonal wurtzite type structure (JCPDS card No. 75-0576). With samarium percentage increments (Fig. 1b–e), the phases obtained by the MH treatment remained ZnO, which indicates the substitution of Sm^{3+} in Zn^{2+} sites. No secondary phase containing Sm was detected, which means that samarium ZnO was incorporated in the network. The absence of deleterious phases indicates the high purity of samples. Figure 1 shows the graph of the three most intense peaks, showing that the zinc oxide is between 30° and 40°. These peaks undergo displacement increases according to the amount of samarium. The intensity of peaks was decreased and the position of peaks shifted slightly towards lower angle with increasing samarium concentration, which indicates that Sm^{3+} doping can cause the expansion of ZnO lattice and decreased the crystalline quality of ZnO [10, 17, 22].

The average crystallite size, lattice parameters and cell volume of ZnO:xSm^{3+} are given in Table 1. The Scherrer equation [25] was used to determine the average crystallite size. The average crystallite size was calculated using the half-height width of the greatest intensity diffraction peaks

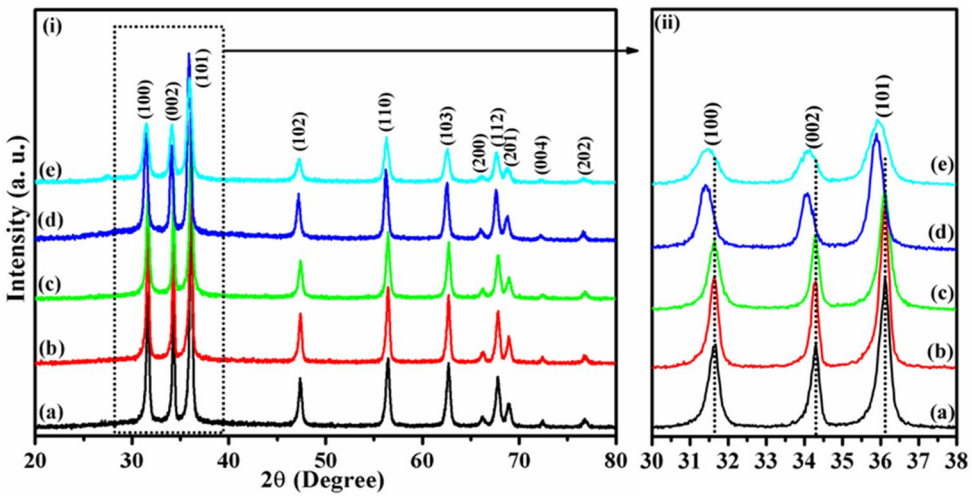

Fig. 1 **i** XRD patterns of ZnO:xSm^{3+} powders prepared by MAH method at 140 °C for 10 min: *a* x = 0, *b* x = 1, *c* x = 2, *d* x = 4 and *e* x = 8 mol%. **ii** *Peaks* (100), (002) and (101) are shown in *inset*

Table 1 Crystal size, Lattice constants (*a* and *c*), and cell volumes (V) of ZnO:xSm^{3+} powders prepared by the MAH method

ZnO:xSm^{3+} (mol%)	Crystal size (nm)	*a* (Å)	*c* (Å)	V (Å)^3
x = 0	31.7	3.290	5.271	49.391
x = 1	26.3	3.283	5.275	49.222
x = 2	26.6	3.290	5.270	49.379
x = 4	21.7	3.300	5.286	49.856
x = 8	15.5	3.302	5.289	49.962

of ZnO, corresponding to (100), (002), (101), (110) and (103) planes. The results in Table 1 show that the average crystallite size decreased with the Sm doping level, from 32 nm for the pure ZnO to 15 nm for 8 mol% Sm^{3+}. The change in the apparent crystallite size of ZnO doped Sm compared to pure ZnO can be attributed to the formation of Zn–O–Sm on the surface of the doped material, which inhibits the growth of crystal grains [23]. The inhibition of the crystallite growth was also observed in doping ZnO with other rare earth [13, 17, 21].

The lattice of wurtzite structure ZnO was calculated, and the results indicate that for Sm-doped ZnO, the lattice parameters were increased, which is expected when zinc clusters [ZnO_6] are substituted by samarium clusters [SmO_6], due to the incompatibility electronic density. The lattice parameters and the cell volume follow a linear relationship with increasing concentration samarium clusters. Thus, the network parameters and the volume increased gradually as the Sm content increased due to repulsive effect of samarium clusters.

Such behavior can be explained by the fact that the increase of Sm doping level was accompanied by an increase in the number of lattice defects. These samarium clusters can cause the formation or reduction of structure defects (oxygen vacancies, distortion on the bonds, stresses and strains on the crystalline lattice) in the materials. Therefore, the dispersion interaction arises from correlation between the electrons situated in the neighborhood of [ZnO_6] and [SmO_6] clusters, effect long-range. These results have shown that the symmetry break process (effect of order–disorder) in the structure of various semiconductors is a necessary condition for the existence of intermediary energy levels within the forbidden gap. These structural changes are related to the polarization at short and medium-range, which can be manifestations of quantum confinement (independently of the particle size). This effect directly influence the band gap semiconductor, increasing its ability to form electron–hole pair stable. As a result, the doped material becomes more active in giving or receiving electrons.

Such behavior is reminiscent of Vegard's law for two-component metal solid solutions, which predicts that the cell dimensions of the solid solution vary linearly with the concentration of the solute component [26]. Expansion in lattice parameters has been observed with decreasing crystallite sizes in many nanocrystalline oxides [27–31].

Figure 2a–e shows ZnO:xSm^{3+} images (x = 0, 1, 2, 4 and 8 mol%). The morphology of both pure and doped ZnO has the form of rods with ends of hexagonal ZnO rods, this hexagonal morphology is a typical feature of the wurtzite structure of hexagonal crystals [19, 32]. It was also observed that this structure has some random growth and bats have holes. Interestingly, as the Sm concentration increases, the appearance of smaller structures is observed, as can be seen in images in Fig. 2a–e. The mechanism of the 3D microrods ZnO:Sm can be proposed. In alkaline condition (pH), Zn^{2+} ions existed in the form of $Zn(OH)_2(H_2O)_4$ complex cluster and $Sm(OH)_3(H_2O)_3$ complex cluster, that was converted to $Zn(OH)_2$ or $Zn(OH)_2{\cdot}xSm(OH)_3$ by precipitation. As a result, irregular ZnO_6 cluster or ZnO_6:xSmO_6 x = 1, 2,

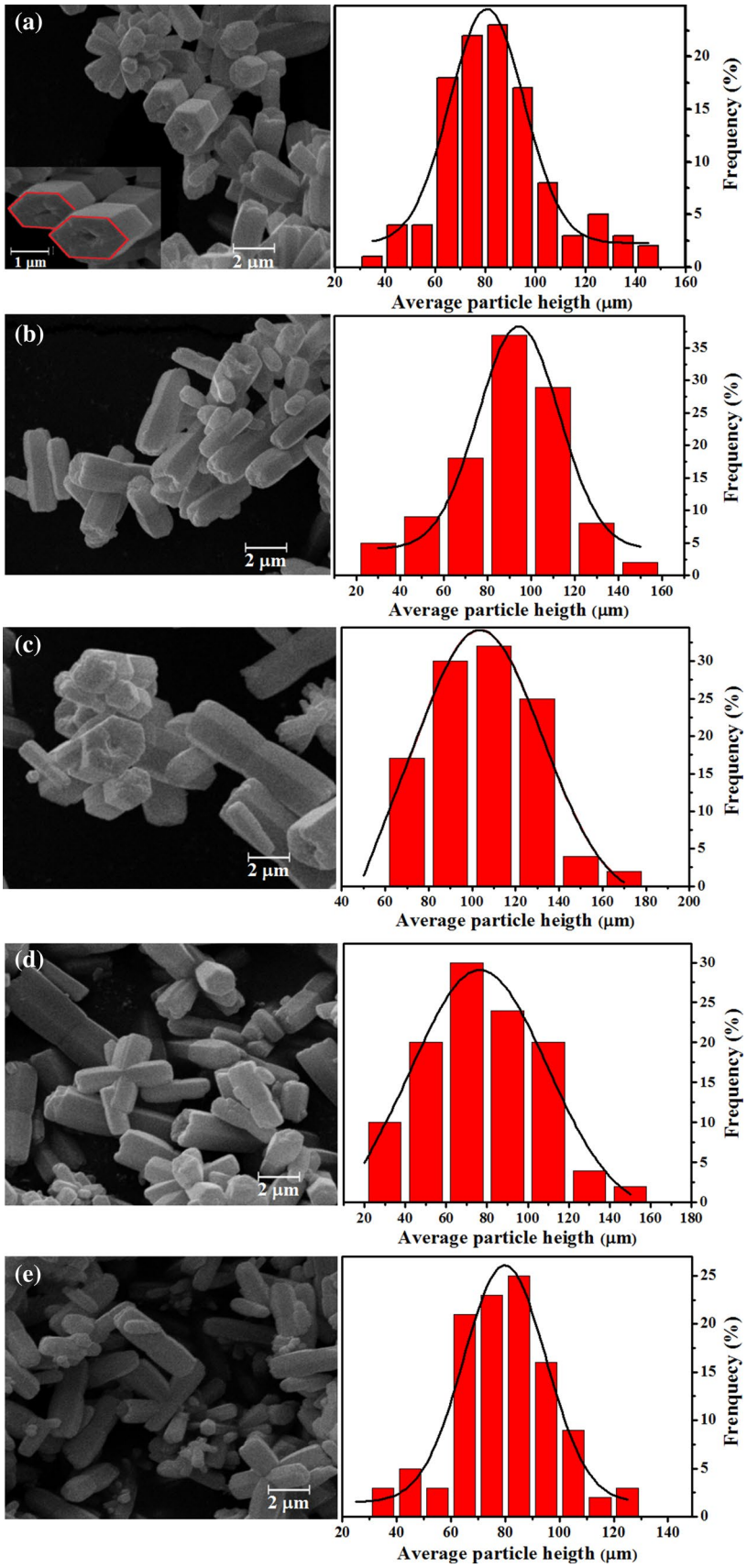

Fig. 2 FE-SEM images and mean particle distributions of ZnO:xSm powders: **a** x = 0, **b** x = 1, **c** x = 2, **d** x = 4 and **e** x = 8 mol%

4, and 8 clusters, that via hydrothermal microwave process is transformed into ZnO or ZnO: m crystals with morphology rods. FEG SEM-image of the products shows that morphology is urchin-like microstructures composed of microrods, pair of microrods and simple microrods.

Huang et al. illustrate the morphology of ZnO nanostructures when synthesized by the hydrothermal method using microwave, which indicates that ZnO nanorods usually develop to the preferred c-axis ([0 2 0] direction) and can be converted into nanowires and nanospindles [20]. Figure 2 shows that the average particle distribution was around 80 μm for pure ZnO and 94, 103, 77 and 80 μm for 1, 2, 4 and 8 mol% Sm^{3+}, respectively.

Samples were also examined by UV–vis diffuse reflectance. Figure 3 shows the optical band gap values as a function of different amounts of Sm^{3+}. The presence of

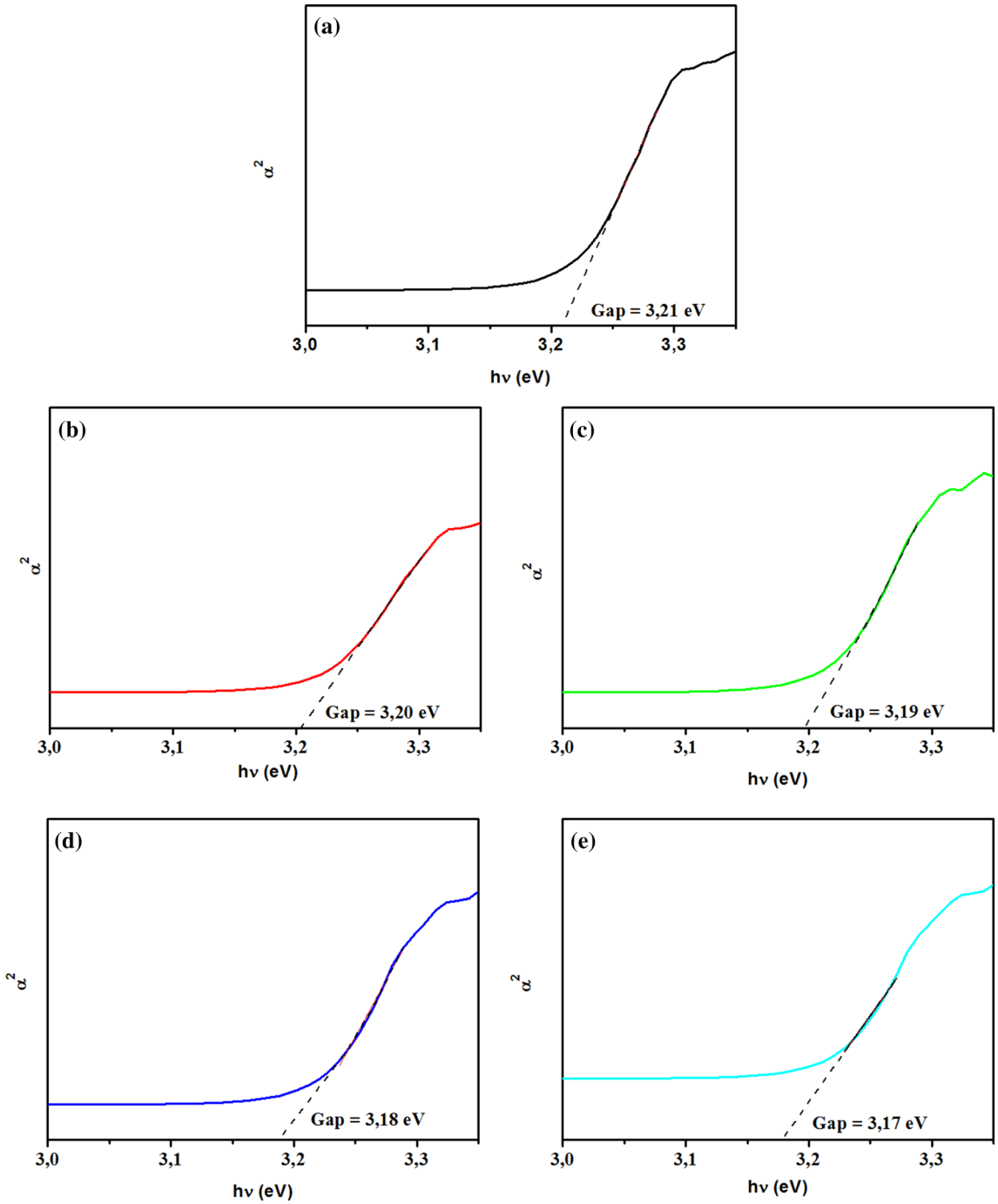

Fig. 3 Effect of Sm concentration on the optical band gap values of ZnO:xSm powders: **a** x = 0, **b** x = 1, **c** x = 2, **d** x = 4 and **e** x = 8 mol%

samarium affecting the ZnO light absorption in the visible range (>400 nm) was higher than that of pure ZnO [17, 22, 23]. It was observed that even with the increased content of Sm, light absorption showed almost the same behavior within the range that corresponds to 450–800 nm. The optical gap estimate was obtained using Wood-Tauc equation [33]. The radiation energy required to carry out the photocatalytic reaction of zinc oxide is about 3.2 eV. The improvement of the catalytic activity appears to be due to the presence of samarium, which tends to generate new band gap energy levels and inhibit the recombination of pairs, increasing the separation speed. The energy gap of the doped product was lower than pure ZnO and is presented in Fig. 3. The results showed that Sm-doped ZnO could be absorbed in the UV region and in the visible region of sunlight. Probably, the reduction in the optical energy gap value may have been generated by replacing Zn ions by Sm ions, inducing the formation of new energy levels in the conduction band or valence [17, 32].

Figure 4a–e shows the emission spectra of ZnO:xSm^{3+} powders at room temperature prepared by the MAH method, λ_{EX} 350.7 nm. The broad and intense band emission covering a large part of the visible spectra (from 400 to 750 nm) can be observed for ZnO:xSm^{3+} particles. Pure ZnO powder displays the most significant PL intensity when excited at this laser beam wavelength (Fig. 4a). The emission spectra of ZnO:xSm^{3+} structures exhibits an efficient red PL emission peak centered at around 600 nm.

The emission band profile is typical of a multiphonon and multilevel process, i.e., a system in which relaxation occurs by several paths involving the participation of numerous states within the band gap of the material [34–37]. This behavior was related to the structural

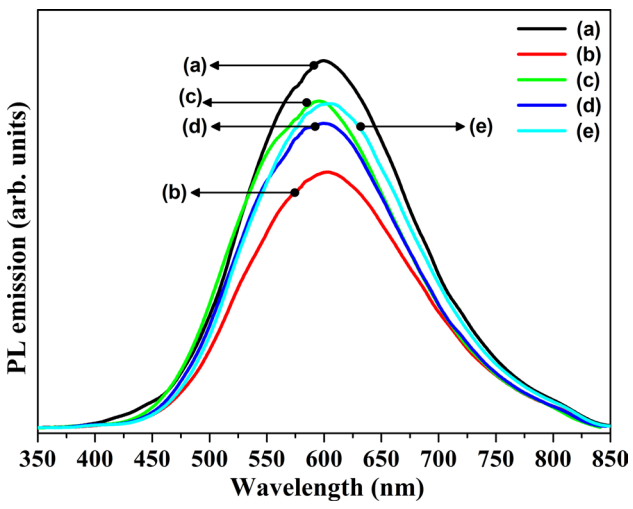

Fig. 4 Photoluminescence emission spectra of ZnO:xSm^{3+} powders prepared using the MAH method: *a* x = 0, *b* x = 1, *c* x = 2, *d* x = 4 and *e* x = 8 mol%

disorder of ZnO and indicates the presence of additional electronic levels in the forbidden band gap of the material.

Electron–hole pairs increase with increasing percentage of Sm in the ZnO structure, which can be confirmed for band gap values calculated for pure ZnO $E_{gap} = 3.21$ and $E_{gap} = 3.17$ eV for 8 mol% Sm^{3+}, exhibiting lower PL intensity. Either pure ZnO or ZnO:Sm belongs to n-type semiconductors, whose oxygen vacancies can induce the formation of new energy levels in the band gap. The generation of oxygen defects in the crystalline structure of cube-like crystals of pure ZnO and ZnO:Sm is apparent.

According to literature, ZnO samples with high amount of oxygen vacancies exhibit high photocatalytic activity [36]. However, they exhibit lower PL intensity, which may result in low recombination rate of electronic electron–hole pairs. Therefore, high amounts of electron–hole pairs may participate in oxidation and reduction reactions and consequently improve the photocatalytic activity.

The catalytic activity of Sm-doped ZnO was evaluated by the degradation of MB dye. Figure 5a shows the photocatalytic activity of ZnO photodegradation without dopant (for comparison), and ZnO doped with 1, 2, 4 and 8 mol% Sm, respectively. As can be seen, all ZnO samples doped with Sm showed higher catalytic activities compared to pure ZnO. The gradual increase in the Sm content enhances the catalytic activity of ZnO samples. The sample showing the best performance on the photodegradation of methylene blue (MB) dye was ZnO with 8 mol% Sm^{3+}, because after 120 min of irradiation, it achieved the highest dye degradation rate. Figure 5b shows the relative ln concentration (C_0/C) versus irradiation time. The behavior experimentally obtained, which is seen in the graph, is the methylene blue of first order behavior in the degradation reaction. The reaction kinetics of MB dye was calculated using equation [22]:

$$\ln\left(C_0/C\right) = kt \tag{2}$$

where C_0 is the concentration before MB irradiation and C is the MB concentration after a certain irradiation time. It was observed that for all experimental results for linear regression of ln data (C/C_0) versus irradiation time, the R^2 value was greater than 0.95 [22].

The cluster-like elucidation of photocatalyst performance is supported by different bulk (intrinsic) and surface (extrinsic) defect distributions, inducing material property changes of the short, medium and long range. The structure defect might be responsible for the different interaction between the semiconductor and the dye material. Effective charge separation (electron/hole) considered in terms of $[ZnO_6]^x_o$ and $[SmO_6]^x_o$ cluster and $[ZnO_6]^x_d$ and $[SmO_6]^x_d$ clusters, where o = order and d = disorder. The intrinsic and extrinsic effect can be considered in terms a hole in the acceptor state and an electron in the donor state are created

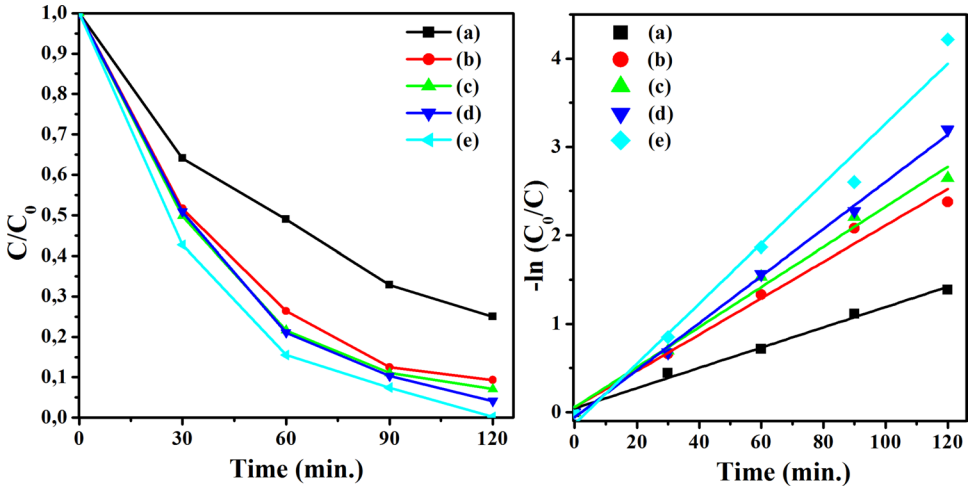

Fig. 5 Effect of different Sm content on MB photodegradation under UV irradiation (254 nm) during different times at 25 °C: *a* x = 0, *b* x = 1, *c* x = 2, *d* x = 4 and *e* x = 8 mol%

according following equations, where the Kröger–Vink notation is used for complex clusters:

$$[ZnO_6]^{x}_{o} + [ZnO_6]^{x}_{d} \rightarrow [ZnO_6]'_{o} + [ZnO_6]^{\cdot}_{d}$$

$$[ZnO_6]'_{o} + [SmO_6]^{x}_{o} \rightarrow [ZnO_6]^{x}_{o} + [SmO_6]^{x}_{o}$$

Thus, there is H_2O and O_2:

$$[ZnO_6]^{\cdot}_{d} + H_2O \rightarrow [ZnO_6]^{x}_{d} + OH^{*} + H^{\cdot}$$

$$[SmO_6]^{\cdot}_{d} + H_2O \rightarrow [SmO_6]^{x}_{d} + OH^{*} + H^{\cdot}$$

$$[ZnO_6]'_{o} + O_2 \rightarrow [ZnO_6]^{x}_{o} + O'_2$$

$$[ZnO_6]'_{o} + O_2 \rightarrow [ZnO_6]^{x}_{o} + O'_2$$

$$O'_2 + H^{\cdot} \rightarrow O_2H^{*}$$

It has been reported in other studies that doping ZnO with lanthanide ions leads to various changes in its physical properties such as band gap and particle size [10–15]. It is known that the catalytic activity of ZnO nanoparticles doped with lanthanide ions is greater than those of pure ZnO [21]. The doping process with lanthanide ions effectively suppresses the electron–hole recombination and produces excessive free radicals necessary for degradation [37]. Table 2 compares the results of this study with previously reported data on the degradation of methylene blue ZnO doped with lanthanide ions.

Table 2 Results found in literature on MB photodegradation

Photocatalyst ZnO doped with:	Experimental conditions			References
	MB (mL)	Catalyst amount (g/L)	Degradation time (min)	
Ho	100	0.15 g	300	[12]
Ni–Th	200	0.375 g	180	[14]
Ce	100	0.4 g	90	[15]
Sm	50	0.05 g	120	This work

4 Conclusion

Pure and samarium-doped zinc oxide with hexagonal shape was prepared using MAH method. XRD analysis showed the single phase with the wurtzite ZnO structure. The SEM results showed that the ends of rods are hexagonal ZnO, which is the typical characteristic of the ZnO hexagonal wurtzite crystal structure. The use of samarium resulted in the reduction of the ZnO band gap. Thus, it showed enhanced absorption of the visible light and consequently, a better catalytic activity, as has been observed in photodegradation tests. The methylene blue dye concentration had a greater reduction by increasing the amount of samarium, and a greater photocatalytic activity was observed with ZnO containing 8% Sm.

Acknowledgements The authors thank the financial support of the Brazilian research financing institutions: CAPES/PROCAD No. 2013/2998/2014, CNPq/Embraer No. 402127/2013-7 and FAPESP 2013/07296-2.

References

1. M. Saif, H. Hafez, A.I. Nabeel, Chemosphere **90**, 840 (2013)
2. J. Miao, Z. Jia, H.-B. Lu, D. Habibi, L.-C. Zhang, J. Taiwan Inst. Chem. Eng. **45**, 1636 (2014)
3. I. Kazeminezhad, A. Sadollahkhani, J. Mater. Sci. **27**, 4206 (2016)
4. N. Jain, A. Bhargava, J. Panwar, Chem. Eng. J. **243**, 549 (2014)
5. K. Hayat, M.A. Gondal, M.M. Khaled, S. Ahmed, A.M. Shemsi, Appl. Catal. A **393**, 122 (2011)

6. C. Karunakaran, V. Rajeswari, P. Gomathisankar, J. Alloy. Compd. **508**, 587 (2010)
7. M.P. Titus, V.G. Molina, M.A. Banos, J. Gimenez, S. Esplugas, Appl. Catal. B **47**, 219 (2004)
8. Z. Zsilák, E. Szabó-Bárdos, O. Fónagy, O. Horváth, K. Horváth, P. Hajós, Catal. Today **230**, 55 (2014)
9. R. John, R. Rajakumari, Nano-Micro. Lett. **4**, 65 (2012)
10. J.-C. Sin, S.-M. Lam, K.-T. Lee, A.R. Mohamed, Ceram. Int. **40**, 5431 (2013)
11. R. Vinodkumar, M.S. Sajna, V.P. Prakashan, N.V. Unnikrishnan, J. Mater. Sci. (2016). doi:10.1007/s10854-016-5467-4
12. A. Phuruangrat, O. Yayapao, T. Thongtem, S. Thongtem, Superlattice Microstruct. **67**, 118 (2014)
13. J.Z. Kong, A.D. Li, H.F. Zhai, Y.P. Gong, H. Li, D. Wu, J. Solid State Chem. **192**, 2061 (2009)
14. Y. Zhou, S.X. Lu, W.G. Xu, Environ. Prog. Sustain. Energy **28**, 226 (2009)
15. K. Vignesh, M. Rajarajan, A. Suganthi, J. Ind. Eng. Chem. **20**, 3826 (2014)
16. M. Faisal, A.A. Ismail, A.A. Ibrahim, H. Bouzid, S.A. Al-Sayari, Chem. Eng. J. **229**, 225 (2013)
17. J.-C. Sin, S.-M. Lam, K.-T. Lee, A.R. Mohamed, Ceram. Int. **39**, 5833 (2013)
18. T. Pandiyarajan, R.V. Mangalaraja, B. Karthikeyan, P. Sathishkumar, H.D. Mansilla, D. Contreras, J. Ruiz, Appl. Phys. A **119**, 487 (2015)
19. C.C. Lin, S.L. Young, C.Y. Kung, L. Horng, H.Z. Chen, M.C. Kao, Y.T. Shih, C.R. Ou, Vacuum **87**, 178 (2013)
20. J. Huang, C. Xia, L. Cao, X. Zeng, Mater. Sci. Eng. B **150**, 187 (2008)
21. M. Khatamian, A.A. Khandar, B. Divband, M. Haghighi, S. Ebrahimiasl, J. Mol. Catal. A **365**, 120 (2012)
22. P.K. Sanoop, S. Anas, S. Ananthakumar, V. Gunasekar, R. Saravanan, V. Ponnusami, Arab. J. Chem. (2012). doi:10.1016/j.arabjc.2012.04.023
23. T. Tsuji, Y. Terai, M.H.B. Kamarudin, M. Kawabata, Y. Fujiwara, J. Non-Cryst. Solids **358**, 2443 (2012)
24. K.D. Bhattea, S.-I. Fujitab, M. Araib, A.B. Panditc, B.M. Bhanage, Ultrason. Sonochem. **18**, 54 (2011)
25. L.V. Azároff, *Elements of X-ray Crystallography* (McGraw-Hill Book Company, New York, 1968), p. 576
26. M.J. McKelvy, R. Sharma, A.V.G. Chizmeshya, R.W. Carpenter, K. Streib, Chem. Mater. **13**, 921 (2001)
27. M.I. Ahmad, S.S. Bhattacharya, Appl. Phys. Lett. **95**, 191906 (2009)
28. S. Tsunekawa, K. Ishikawa, Z.-Q. Li, Y. Kawazoe, A. Kasuya, Phys. Rev. Lett. **85**, 3440 (2000)
29. P. Ayyub, V.R. Palkar, S. Chattopadhyay, M. Multani, Phys. Rev. B **51**, 6135 (1995)
30. A. Cimino, P. Porta, M. Valigi, J. Am. Ceram. Soc. **49**, 152 (1966)
31. G. Li, J.B. Goates, B.F. Woodfield, L. Li, Appl. Phys. Lett. **85**, 2059 (2004)
32. J.-C. Sin, S.-M. Lam, K.-T. Lee, A.R. Mohamed, J. Colloid Interface Sci. **401**, 40 (2013)
33. D.L. Wood, J.S. Tauc, Phys. Rev. B **5**, 3144 (1972)
34. F.V. Motta, A.P.A. Marques, M.S. Li, M.F.C. Abreu, C.A. Paskocimas, M.R.D. Bomio, R.P. Souza, J.A. Varela, E. Longo, J. Alloy. Compd. **553**, 338 (2013)
35. M.T.S. Tavares, L.X. Lovisa, V.D. Araújo, E. Longo, M.S. Li, R.M. Nascimento, C.A. Paskocimas, M.R.D. Bomio, F.V. Motta, Mater. Sci. Semicond. Process. **27**, 1036 (2014)
36. X. Liun, W. Huangnn, G. Huang, F. Fu, H. Cheng, W. Guo, J. Li, H. Wu, Ceram. Int. **41**, 11710 (2015)
37. R. Kumar, A. Umar, G. Kumar, M.S. Akhtar, Y. Wang, S.H. Kim, Ceram. Int. **41**, 7773 (2015)